Author(s): Kozulin, E. M.; Knyazheva, G. N.; Itkis, I. M.; Itkis, M. G.; Bogachev, A. A.; Chernysheva, E. V.; Krupa, L.; Hanappe, F.; Dorvaux, O.; Stuttgé, L.; Trzaska, Wladyslaw; Schmitt, C.; Chubarian, G.

Title: Fusion-fission and quasifission of superheavy systems with Z=110-116 formed in 48Ca-induced reactions

Year: 2014

Version:

Fusion-fission and quasifission of superheavy systems with $Z = 110$–116 formed in ^{48}Ca-induced reactions

E. M. Kozulin, G. N. Knyazheva, I. M. Itkis, M. G. Itkis, A. A. Bogachev, E. V. Chernysheva, and L. Krupa
Flerov Laboratory of Nuclear Reactions, Joint Institute for Nuclear Research, 141980 Dubna, Moscow Region, Russia

F. Hanappe
Université Libre de Bruxelles, CP229, B-1050, Belgique

O. Dorvaux and L. Stuttgé
Institut Pluridisciplinaire Hubert Curien and Université de Strasbourg, F-67037 Strasbourg, France

W. H. Trzaska
Department of Physics, University of Jyvä skylä, P.O. Box 35 (YFL), FI-40014 Jyväskylä, Finland

C. Schmitt
GANIL, Bd. Henri Becquerel, BP 55027, F-14076 Caen Cedex 05, France

G. Chubarian
Cyclotron Institute, Texas A&M University, College Station, Texas 77843, USA

Background: In heavy-ion-induced reactions the mechanism leading to the formation of the compound nucleus and the role of quasifission is still not clear.

Purpose: Investigation of the quasifission process of superheavy composite systems with $Z = 110$-116 and comparison with properties of fusion-fission and quasifission of lighter composite systems.

Method: Mass and energy distributions of fissionlike fragments formed in the reactions ^{48}Ca +^{232} Th, ^{238}U, ^{244}Pu, and ^{248}Cm at energies near the Coulomb barrier have been measured using the double-arm time-of-flight spectrometer CORSET at the U-400 cyclotron of the FLNR JINR.

Results: The most probable fragment masses as well as total kinetic energies and their dispersions in dependence on the interaction energies and ion-target combinations have been studied for asymmetric and symmetric fragments formed in the reactions. The capture cross sections were obtained for the reactions ^{48}Ca +^{244} Pu and ^{248}Cm. The lower limits for fission barriers of $^{283-286}$Cn, $^{289-292}$Fl, and $^{293-296}$Lv compound nuclei were estimated.

Conclusions: Analysis of the properties of symmetric fragments has shown that a significant part of these fragments may be attributed to fusion-fission process for the reactions ^{48}Ca+^{238}U, ^{244}Pu, and ^{248}Cm.

I. INTRODUCTION

In the last decade a great success was achieved in the synthesis of superheavy elements with $Z = 112$–118 bombarding actinide targets with ^{48}Ca ions. In these reactions the fusion-evaporation cross sections are larger than in the case of cold-fusion reactions and are of the order of a few picobarns [1]. Nevertheless, even in the case of Ca-induced reactions, the composite system formed after capture can break apart into two fragments again via the quasifission process (QF) before the system reaches the compact configuration below the fission barrier of compound nucleus (CN).

Both the CN fission and the QF are characterized by large nucleon exchange and energy dissipation making the distinction between the two processes difficult, especially in the case of a symmetric mass split.

Today the properties of fission of nuclei up to the element with $Z = 106$ are well investigated. It was found that in spontaneous and low-energy fission a dominant role in the formation of fission fragments is played by the spherical nuclear shells with $Z = 50$ and $N = 82$ and deformed neutron shell at $N = 88$ [2]. The fission of nuclei at excitation energies higher than 40 MeV (where the influence of shell effects is negligible) is well described by the liquid drop model (LDM) and characterized by symmetric Gaussian-like shape mass and energy distributions. The properties of fragment mass and energy distributions in the case of fission of hot nuclei were summarized in Ref. [3] in dependence on the CN temperature and angular momentum for a wide range of nuclei up to $Z = 104$.

Nowadays several theoretical approaches to describe the dynamics of heavy-ion-induced reactions were developed. Note that the theoretical models describing the fission process in terms of diffusion over a complicated multidimensional potential energy surface can reliably predict the properties of fission fragments [4–6]. However, the predictions of theoretical approaches, for example [7–9], applied to describe the whole evolution of low-energy nucleus-nucleus collision at strong channel coupling of deep-inelastic scattering, CN formation, and QF, differ from each other by several orders

of magnitude and experimental data are needed to define the constants used in these models.

In systematic studies of quasifission process using ^{238}U and ^{208}Pb beams incident on targets ranging from ^{16}O to ^{89}Y [10,11] was found that in superheavy composite systems QF is a dominant process leading to the formation of asymmetric fragments with mass asymmetry ~0.4. This type of QF process, the so-called asymmetric quasifission (QFasym), is characterized by asymmetric angular distributions in the center-of-mass system and thus associated with fast reaction times (10^{-21}s = 1zs) [12], faster than CN fission (larger than 10 zs). Besides the asymmetric component, the symmetric one may also be affected by the presence of the QF process (QFsym). The characteristics of angular K distribution may also be different for CN fission and QF due to the fact that only CN fission passes through the true saddle point [13]. Indeed, it has been found that angular anisotropies for QF are significantly larger than those for fusion-fission reactions.

Many studies on mass and angular distributions for different reactions have been done since the discovery of QF about 30 years ago. In these investigations the main attention was paid to the fusion probabilities [12,14,15] and fusion-fission properties. Many efforts have been also done in the investigations of mass-angle correlations of QF fragments in order to estimate the time scale of heavy-ion-induced reactions [10–16]. Nevertheless at present there is no systematic data on QF fragment properties, such as fragment mass and energy distributions as a function of incident energy and target-ion combination.

The study of mass and energy distributions of binary fragments obtained in the reactions of ^{48}Ca ions with the ^{232}Th, ^{238}U, ^{244}Pu, and ^{248}Cm at energies below and above the Coulomb barrier will be presented. The properties of mass and TKE of QF fragments in dependence on interaction energy have been investigated and compared with characteristics of the CN-fission process.

II. EXPERIMENTAL DETAILS

The experiments were carried out at the Flerov Laboratory of Nuclear Reactions using beams of ^{48}Ca ions from the U-400 cyclotron at energies around the Coulomb barrier. Beam energy resolution was about 1% and intensities were in the range of 2–3 pnA. Layers of ^{232}Th, ^{238}U, ^{244}Pu, and ^{248}Cm, 180–220 μg/cm^2 thick, deposited on a 40–50 μg/cm^2 carbon backing, were used as targets. The ^{248}Cm target (125 μg/cm^2) was sputtered on ^{27}Al backing (20 μg/cm^2) and covered on both sides by carbon ^{12}C (40 μg/cm^2). The enrichment was 99.99%.

Binary reaction products were detected in coincidence by the double-arm time-of-flight spectrometer CORSET [17]. Each arm of the spectrometer consists of a compact start detector and an assembly of four position-sensitive stop detectors, based on microchannel plates. The start detectors were placed at a distance of 4 cm from the target. The distance between the start and stop detectors was 14 cm. Thus the angular acceptance for both arms was $\pm18°$ in plane and $\pm12°$ out of plane. The arms of the spectrometer were positioned symmetrically at the angles of $60°$ to the beam axis. With this

choice of angles, the scission axis is orthogonal to the beam axis for the case of symmetric splitting. In other words, the fragments were detected at $90°$ in the center-of-mass system. The position resolution of the stop detectors was $0.3°$ and the time resolution was about 150 ps. The typical mass resolution of the spectrometer in these conditions was ±1.5 u and the energy resolution was $\pm2\%$.

The data processing assumed standard two-body kinematics [17]. Primary masses, velocities, energies, and angles in the center-of-mass system of reaction products were calculated from measured velocities and angles in the laboratory system using the momentum and mass conservation laws with the assumption that the mass of the composite system is equal to $A_t + A_p$, A_t, and A_p are the masses of target and projectile, respectively. Neutron evaporation before scission was not taken into account. This is justified by the fact that even at the highest reaction energies not more than four neutrons could be emitted. Hence, considering that the spectrometer resolution is 2–3 u, the neutron emission will not lead to visible effects on the mass-energy distributions. Fragment energy losses in the target, backing, and the start detectors foils were taken into account.

The identification of the binary reaction channel with full momentum transfer (FMT) and the removal of products of sequential and incomplete fission reactions, induced fission of target and targetlike nuclei, or from reactions on impurity atoms in the target was based on the analysis of the kinematic diagram (the velocity vectors of two detected reaction products) in the center-of-mass system [17]. For FMT events the distribution of the $V_\perp$ component of fragment velocity (projection of the fragment velocity vector onto the plane perpendicular to the beam) is expected to peak at zero, while the $V_\parallel$ (projection of the fragment velocity vector onto the beam axis) should be equal to the calculated center-of-mass velocity for the collision $V_{c.m.}$.

III. RESULTS

The entrance channel properties of investigated reactions are presented in Table I.

Mass-total kinetic energy (M-TKE) distributions of the primary binary fragments obtained in the reactions ^{48}Ca + ^{232}Th, ^{238}U, ^{244}Pu, and ^{248}Cm are shown in Fig. 1. The distributions in Fig. 1 are presented at energies below and above the Coulomb barrier. In the M-TKE distribution the reaction products with masses close to those of the projectile and target are associated with quasielastic and deep-inelastic events. They were not considered in the present analysis. Since the measurements have been done at energies around the barrier, the grazing angles for the studied systems are close to $180°$ (see Table I). Therefore the contribution of deep-inelastic events is insignificant. Reaction products located between quasielastic peaks are assumed as totally relaxed events, i.e., as fissionlike fragments, and can originate either from CN-fission or QF processes. The events selected are those within the rectangles in the M-TKE distributions in Fig. 1. The mass-energy distributions are similar for all the reactions. The clearly pronounced asymmetric QF component with heavy fragments near the double magic lead is observed.

TABLE I. Properties of the systems investigated in this paper. E_{lab} is the projectile energy. $\theta_{lab}^{grazing}$ is the grazing angle in the laboratory system [18]. $\eta_0 = (A_t - A_p)/(A_t + A_p)$ is the entrance channel mass asymmetry. β_{target} is the deformation parameter for target nuclei, as deduced from the electric quadrupole transition probability between the first 2^+ state and 0^+ ground state [19]. E_{Bass} is the Bass barrier in the center-of-mass system [18].

Reactions	E_{lab}, MeV	$\theta_{lab}^{grazing}$, deg	η_0	$Z_p Z_t$	β_{target}	E_{Bass}, MeV
^{48}Ca $+^{232}$Th $\rightarrow ^{280}$Ds	244	106	0.6571	1800	0.2608	190.37
^{48}Ca $+^{238}$U $\rightarrow ^{286}$Cn	228–238	171–123	0.6643	1840	0.2863	193.84
^{48}Ca $+^{244}$Pu $\rightarrow ^{292}$Fl	226–244	180–118	0.6712	1880	0.2931	197.29
^{48}Ca $+^{248}$Cm $\rightarrow ^{296}$Lv	233–240	180–138	0.6757	1920	0.2972	201.08

In the reactions with heavy ions the capture takes place if the initial energy of the projectile in the center-of-mass system is enough to overcome the Coulomb barrier and consequently the capture cross section is a sum of the QF, CN-fission, and evaporation residue (ER) cross sections. For the studied reactions the cross section of the evaporation residues is approximately a few picobarns [1] and contributes insignificantly to the fusion cross section, i.e., in formation of CN.

It is important to note that in the studied reactions all target nuclei are well deformed. Reaction dynamics of deformed nuclei strongly depends on the relative orientation of the reaction partners, which changes the Coulomb barrier and the distance between the centers of the colliding nuclei. When two interacting nuclei touch each other by their lateral surfaces (near-side collisions), a high formation probability of a spherical CN is expected, whereas in the elongated configuration, when nuclei touch each other by their poles

(near-tip collision), a high QF probability is expected. In Fig. 2 the mass-energy distributions for the reactions ^{48}Ca $+^{144}$Sm and ^{48}Ca $+^{208}$Pb (targets and projectiles are spherical) and for the reactions ^{48}Ca $+^{154}$Sm and ^{48}Ca $+^{238}$U (both targets are strongly deformed) at energy near the Coulomb barrier are shown [20–22]. It is clearly seen that in the case of spherical interacting nuclei the mass distributions exhibit a nearly Gaussian shape typical for CN fission whereas in the reactions with deformed targets the asymmetric QF is well pronounced, as in the reaction leading to superheavy composite system, as well as in the reaction leading to moderately fissile compound nucleus, for which the yields of fission and ER production are comparable. As it was shown in Ref. [23], the presence of entrance-channel magicity (the number of spherical shells in the reaction entrance channel) reduces QF. The QF reaction channels that are characterized by the formation of fragments with highly asymmetric mass
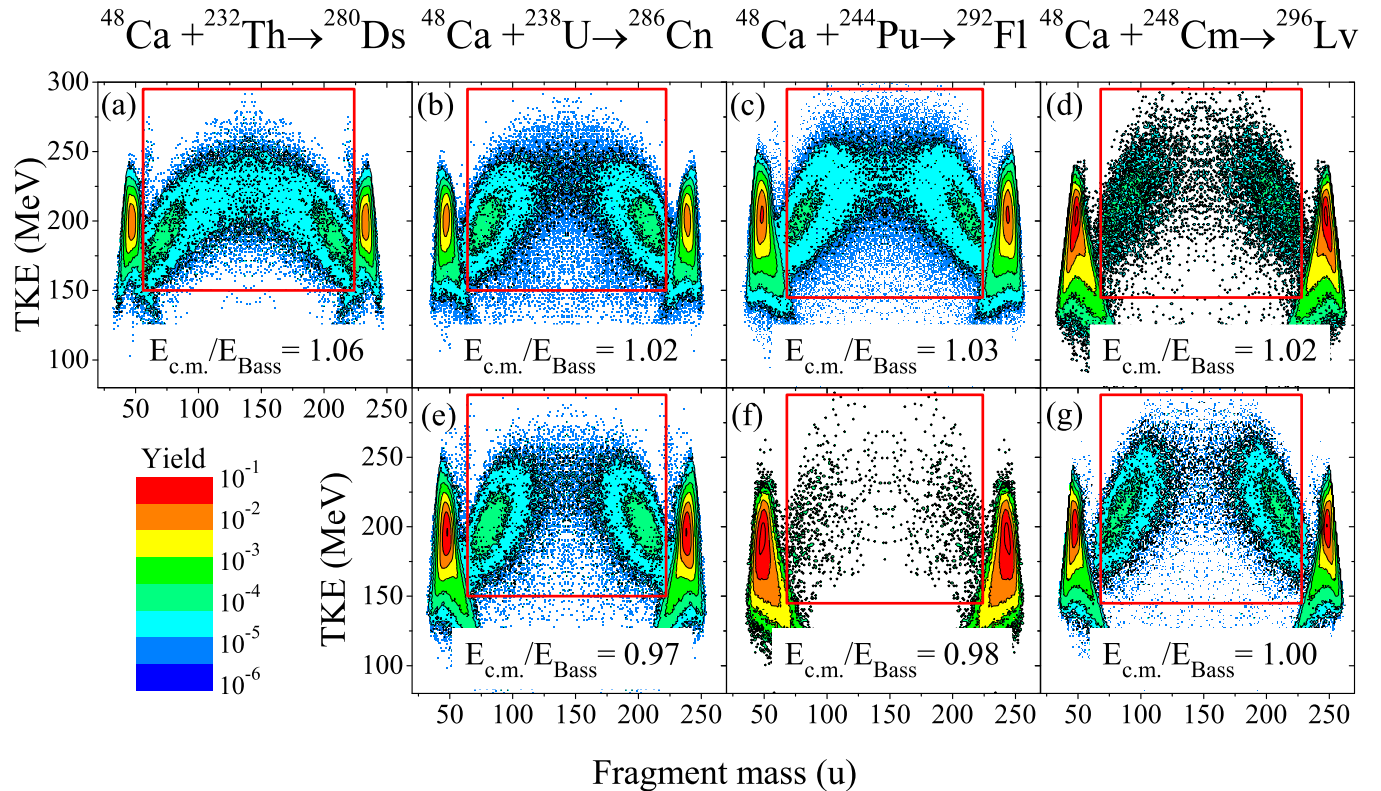

FIG. 1. (Color online) Mass-energy distributions of fragments obtained in the reactions ^{48}Ca $+^{232}$Th, ^{238}U, ^{244}Pu, ^{248}Cm at energies above (top) and below (bottom) the Bass barrier. The red rectangles indicate the gates used to select fissionlike events.
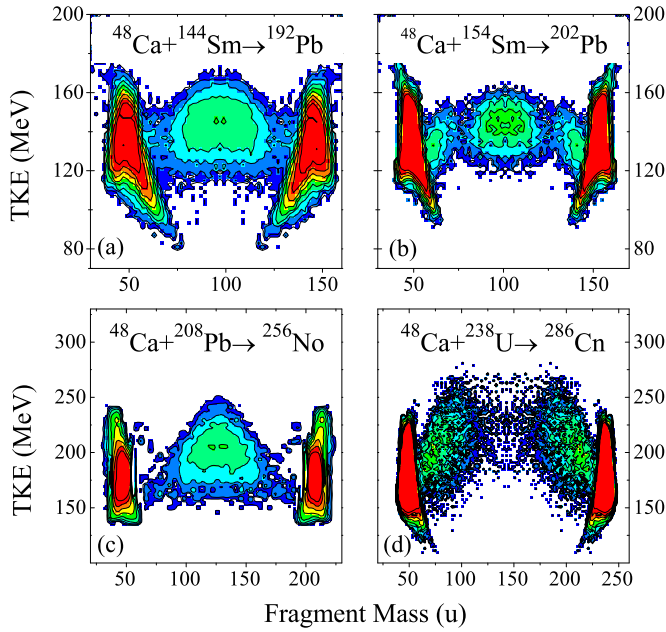
FIG. 2. (Color online) Mass-energy distributions of fragments obtained in the reactions ^{48}Ca $+^{144}$Sm (a) and ^{48}Ca $+^{208}$Pb (c) (target and projectile are spherical) in comparison with the reactions ^{48}Ca $+^{154}$Sm (b) and ^{48}Ca $+^{238}$U (d) (targets are strongly deformed) at energy near the Coulomb barrier.

division (QFasym) most probably occur at the earliest stage of the collective motion, when the composite system is still strongly deformed. We have to stress that the QFasym is the result of the action of different nuclear shells for different composite systems: for composite systems with $Z \sim 80$ the shells with $Z = 28, 50$ and $N = 50, 82$ play that role, while for superheavy composite systems the shells at $Z = 28, 82$ and $N = 50, 126$ are responsible. Nevertheless, we observe symmetric fragments in all the measured M-TKE distributions of fissionlike fragments formed in the reactions ^{48}Ca $+^{232}$Th, ^{238}U, ^{244}Pu, and ^{248}Cm. These symmetric fragments may be formed in CN-fission process as well as in quasifission.

IV. MASS DISTRIBUTIONS

The mass distributions of the fissionlike fragments inside the rectangular gates in Fig. 1 integrated over all kinetic energies are presented in Fig. 3. The spectra are normalized in such a way that the total area of each spectrum integrated over the mass range yields 200%. As it was already mentioned the mass distributions have a wide two-humped shape with the light QF fragments mass distribution extending from 55 u to 115 u. For these reactions the driving potentials as a function of mass asymmetry and distance between mass centers have been calculated in the diabatic approximation using the proximity model with the help of nuclear reaction vision project (NRV) [18]. These potentials are shown in the top panel of Fig. 3.

Some noteworthy features of the QFasym fragments mass distributions can be highlighted at this point. Generally, in heavy-ion-induced reactions the formation of QFasym

fragments is connected with the strong influence of the nuclear shell at $Z = 82$ and $N = 126$ (double magic lead). In fact for the ^{48}Ca $+^{232}$Th and ^{48}Ca $+^{238}$U reaction the maximum yield corresponds to fragments with masses around 208 u. However, in reactions with heavier targets the maximum is shifted from 208 u up to 211 u for the reaction ^{48}Ca $+^{248}$Cm. Notice, for the reaction ^{64}Ni $+^{238}$U, the maximum yield of QFasym fragments corresponds to the heavy mass 215 u [22]. As it was shown in Ref. [24] the shells in light fragment at $Z = 28$ and $N = 50$ could be effective, together with the shell $Z = 82$ and $N = 126$, and could lead to the shift of the asymmetric QF peak. According to the driving potential the position of the minimum is shifted from 206 u for the reaction ^{48}Ca $+^{232}$Th up to 211 u for the reaction ^{48}Ca $+^{248}$Cm. The calculated position of the minimum of the driving potential agrees with the position of peaks in the experimental QFasym mass distributions (see arrows in Fig. 3).

Besides the position of peaks in the mass distributions of QFasym fragments, also the widths of these peaks vary for different ion-target combinations. Figure 4 presents the drift to the mass symmetry of QFasym (estimated as a difference between the mass with maximum yield and more symmetric mass at half maximum yield) as a function of the energy above the Bass barrier for the reactions ^{48}Ca $+^{232}$Th, ^{238}U, ^{244}Pu, and ^{248}Cm. At energies below the Bass barrier the maximum drift is observed for the reaction with ^{248}Cm target, the minimum for ^{238}U and ^{244}Pu lies between these reactions. It is clearly seen that the deepest narrow minimum in driving potential at mass close to 208 u corresponds to the reaction ^{48}Ca $+^{238}$U that is the case of the narrowest QFasym mass distribution, for the reaction with ^{244}Pu this minimum is wider and for ^{248}Cm is the widest.

The drift toward mass symmetry increases with collision energy up to the barrier energy. At energy above the barrier the width of QFasym does not change anymore. Also for higher energy the estimation of the width of QFasym is not longer possible due to the growing yield of symmetric fragments that start to dominate at these energies.

The increasing drift toward mass symmetry of QF with the increasing collision energy has been observed previously in the reactions with ^{238}U ions [10]. In this work the mass-energy and angular distributions of QF fragments have been measured and the time scale for mass transfer in QF reactions has been derived from rotation angles of the composite system. It has been found that the mass drift toward symmetry shows the characteristics of an overdamped motion with a universal time constant independent of scattering system and bombarding energy. It indicated that the drift toward mass symmetry occurs as overdamped motion given by [10]:

$$\frac{\Delta A}{\Delta A_{\max}} = \frac{A_p - \langle A \rangle}{\frac{1}{2}(A_t - A_p)} = 1 - \exp[-(t - t_0)/\tau], \quad (1)$$

where $\tau = (5.3 \pm 1)$ zs is the time constant common to all systems, $t_0 \sim 1$ zs is a time delay before mass drift sets in. According to Fig. 4 the widths of QFasym at energies above the barrier are similar for all studied reactions with the ratio of $\Delta A / \Delta A_{\max} \approx 0.66$. When the collision energy increases the shell effects decrease and the differences in the depth of
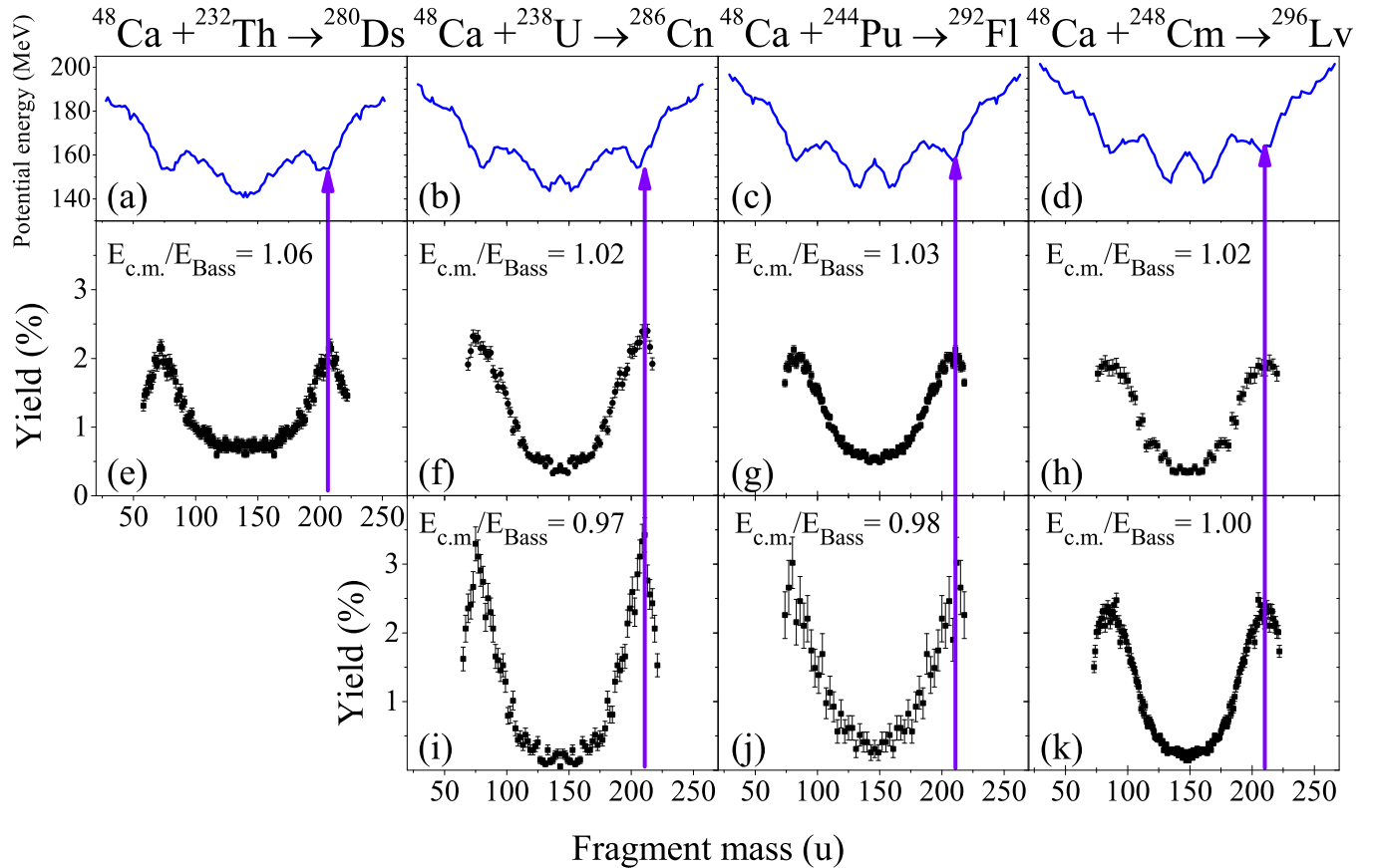
FIG. 3. (Color online) Potential energies at contact configuration (top panel) and experimental mass distributions of fissionlike fragments formed in the reactions ^{48}Ca $+^{232}$Th,^{238}U,^{244}Pu,^{248}Cm: at energy above (middle) and below (bottom) the Bass barrier.

the minimum responsible for QFasym process in the potential energies for the studied systems become negligible, while at energies slightly above the barrier the shell effects are still quite visible. According to Eq. (1) to reach this drift toward mass symmetry composite system should live around 6.7 zs and for QFasym process in the reactions with ^{48}Ca ions the interaction
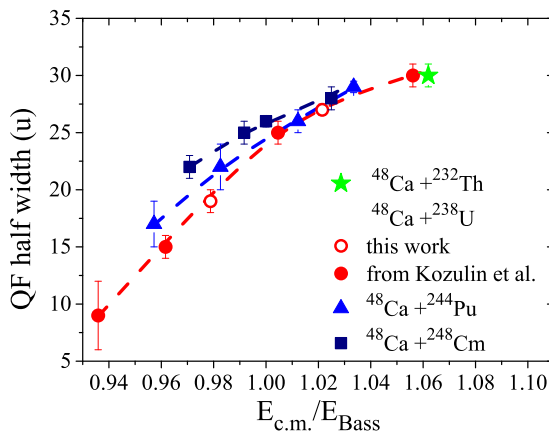

FIG. 4. (Color online) The widths of QFasym mass distributions as a function of the energy above the Bass barrier for the reactions ^{48}Ca $+^{232}$Th,^{238}U,^{244}Pu, and ^{248}Cm. The solid circles are taken from Ref. [22] for the ^{48}Ca $+^{238}$U reaction.

time does not depend on the reaction entrance channel. However, for more symmetric reactions, such as, ^{58}Fe $+^{244}$Pu ($Z_p Z_t = 2444$) and ^{64}Ni $+^{238}$U ($Z_p Z_t = 2576$), leading to the formation of a similar composite system ^{302}120, the mass drift to the symmetry is 22 nucleons in the case of the ^{58}Fe reaction at $E_{c.m.}/E_{Bass} = 1.04$ and only 11 nucleons in the case of the ^{64}Ni ion at $E_{c.m.}/E_{Bass} = 1.06$ [25]. Thereby, in the reactions with ^{48}Ca the interaction time for QFasym process virtually does not change, while for heavier reactions it decreases up to about 5 zs in the case of ^{58}Fe reaction and 3.6 zs in the case of ^{64}Ni reaction.

As a first step to evaluate the CN-fission cross section the contribution of fragments with masses $A_{CN}/2 \pm 20$ u can be considered. We may expect that the mass distributions of the CN-fission fragments can have the symmetric Gaussian shape with the standard deviation of about 20 u (see for example Ref. [24] for the case of Hs ($Z = 108$) nucleus), as predicted by the LDM, or asymmetric shape caused by the influence of the closed shells with $Z = 50$ and $N = 82$ as in the case of fission of actinides elements [26]. But in both cases the width of CN-fission fragment mass distributions does not exceed 40 u and the choice of the mass range of $A_{CN}/2 \pm 20$ u is reasonable.

The relative contributions of fragments with masses $A_{CN}/2 \pm 20$ u into the capture cross section (fragments inside the rectangles in the M-TKE distributions in Fig. 1)
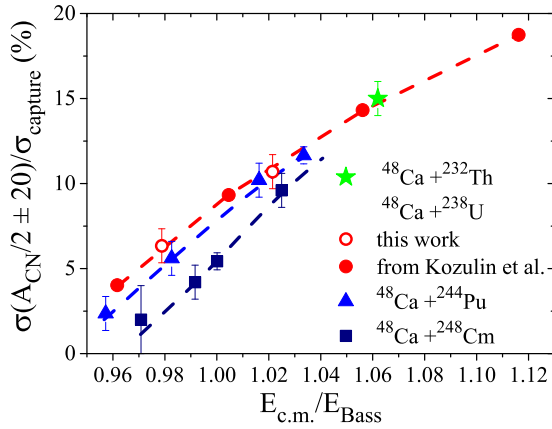
FIG. 5. (Color online) The contributions of symmetric fragments to the capture cross sections for the studied systems as a function of energy above the barrier. The solid circles are taken from Ref. [22] for the ^{48}Ca $+^{238}$ U reaction.
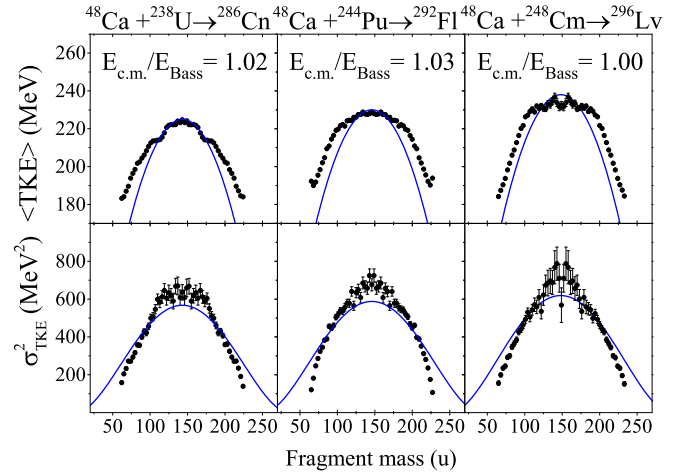

FIG. 6. (Color online) Average total kinetic energy (top) and its dispersion (bottom) as a function of mass for fissionlike fragments formed in the reactions ^{48}Ca $+^{238}$ U,^{244}Pu, and ^{248}Cm at energies slightly above the Bass barrier.

for the reactions of ^{48}Ca-ion with ^{232}Th, ^{238}U, ^{244}Pu, and ^{248}Cm are shown in Fig. 5. The contribution of symmetric fragments increases with increasing collision energies for all studied systems. In the recent paper of Nishio [27] the mass distributions for the reaction ^{48}Ca $+^{238}$ U have been measured up to the energy of 20% above the barrier. For this energy ($E_{\text{c.m.}}/E_{\text{Bass}} = 1.27$) the mass distribution is mainly symmetric. At energies below the barrier the contribution of symmetric fragments decreases at the transition from ^{238}U to ^{248}Cm. The contribution of symmetric fragments is about 6% for ^{238}U, 5% (within the error bar approximately the same as for ^{238}U) for ^{244}Pu and only 2.5% (more than twice less) for ^{248}Cm at $E_{\text{c.m.}}/E_{\text{Bass}} = 0.98$. The average interaction time depends on the reaction entrance channel. The decreasing contribution of symmetric fragments at energies below the barrier for the case of ^{244}Pu and ^{248}Cm may result from smaller average interaction time compared with reaction ^{48}Ca $+^{238}$ U due to increased the Coulomb repulsion. At energies above the barrier the yields of symmetric fragments are similar for all reactions under study. The increasing collision energy leads to stronger overlapping of interacting nuclei surfaces and consequently to larger interaction time.

V. ENERGY DISTRIBUTIONS

The energy characteristics of the fissionlike products are directly connected to the shape of the dinuclear system and the distance between the centers of nascent fragments in the scission point, as the kinetic energy is mainly defined by the Coulomb repulsion at the scission point. In fission process of heated nuclei at $E^* > 40$–50 MeV, when the shell effects are dumped, the average kinetic energy has a parabolic dependence on the fragment mass and virtually does not depend on the excitation energy and angular momentum of the CN. Such behavior of the TKE is confirmed by experimental data [3]. The most probable TKE of CN fission increases with increasing the $Z_{\text{CN}}^2/A_{\text{CN}}^{1/3}$ parameter and the value of $\langle$TKE$\rangle$ can be estimated with the Viola systematics [28].

Another important feature connected with the dynamics of the dinuclear system (transition stage from saddle to scission) is the dispersion of the TKE of the formed fragments. In fact the compilation of the experimental data at excitation energies of the CN of $\sim$40–50 MeV [3] shows that the TKE dispersion practically does not change for compound nuclei with $Z_{\text{CN}}^2/A_{\text{CN}}^{1/3}$ up to $\sim$1000 (where saddle and scission points are close to each other) and increases linearly for heavier CN (long transition between saddle and scission points). According to this systematics, values of $\sim$500 MeV^2 for the TKE dispersion are expected for these compound nuclei.

In Fig. 6 the experimental $\langle$TKE$\rangle$ and σ_{TKE}^2 measured in this work are displayed as a function of the fragment mass for ^{48}Ca on ^{238}U, ^{244}Pu, and ^{248}Cm at above barrier energies. Solid curves are the descriptions of the LDM component with the parameters from [29]. In the case of ^{48}Ca $+^{238}$ U and ^{244}Pu the average TKE for symmetric fragments exhibits a parabolic dependence, while for the reaction with ^{248}Cm there is a structure and the average TKE is lower than predicted values. The deviations from the parabolic shape become significant for QF fragments with masses greater than 175 u. For the masses $M = 200$–210 u (mass-asymmetry for these fragments is $\eta \approx 0.40$–0.45) the experimental value of $\langle$TKE$\rangle$ is higher by 10–15 MeV than the LDM prediction.

The same trend for QF fragments has been observed in the reactions ^{48}Ca $+^{154}$ Sm,^{170}Er [20,30] leading to the lighter composite systems of ^{202}Pb and ^{218}Th. In these reactions the $\langle$TKE$\rangle$ for QF fragments with mass asymmetry $\eta \approx 0.35$–0.40 is higher by 7–15 MeV than expected for the fission fragments at the same mass asymmetry. Since QFasym is strongly influenced by the shell effects, the composite system holds a more compact shape at scission resulting in higher $\langle$TKE$\rangle$ as compared with the predictions of the LDM model. It should be noted that in the fission of actinide nuclei the TKE of the fission fragments may also be higher than the LDM value due to the modal fission caused by the shell effects [31].

Deviations from the predicted values are also observed in TKE dispersions. As it was shown in Ref. [24] the dispersion of TKE as a function of fragment mass agrees with the prediction in the case of fission of Hs, obtained in the reactions ^{22}Ne $+^{249}$Cf and ^{26}Mg $+^{248}$Cm, while in the case of the ^{58}Fe $+^{208}$Pb, where the main process is QF, the experimental dispersion is much lower than predicted. In the case of the reaction ^{36}S $+^{238}$U both CN fission and QF contribute significantly in the symmetric fragment region, and the dispersion of TKE is higher than predicted for the symmetric fragment masses and is lower for QFasym fragments. As it is clearly seen from Fig. 6 the experimental TKE dispersions for the reactions ^{48}Ca $+^{238}$U, ^{244}Pu, and ^{248}Cm at energies near the Bass barrier behave similarly to the ^{36}S $+^{238}$U reaction. By analogy with modal fission the increase of TKE dispersion may indicate the presence of several independent processes leading to the formation of symmetric fragments. It is known that for heavy composite systems formed in the reaction with heavy ions the QFasym process dominates at energies below the Bass barrier and the contribution of symmetric fragments into all fissionlike fragments grows with increasing interaction energy. This rise may be caused by CN fission, but also by QFsym. At the same time, the increase of projectile energy leads to mass drift of quasifission toward the symmetry, making difficult the distinction between CN-fission and QF events based on mass-energy distributions alone. However, the large value of TKE dispersion for symmetric mass region indicates the simultaneous presence of different processes, namely, CN fission, QFasym, and QFsym.

Figure 7 shows the average TKE as a function of the energy above the Bass barrier for symmetric ($A_{CN}/2 \pm 20$ u) and asymmetric (for the fragment mass where the yield of QFasym is maximal) fragments for the reaction ^{48}Ca $+^{238}$U. We also include the data from Ref. [22] where the measurements have been done with CORSET spectrometer in a wider collision energy region. For the symmetric fragments the TKE increases with interaction energy: at energies below the Bass barrier

FIG. 8. (Color online) Average TKEs for asymmetric QF (corresponding to the QFasym fragments with the maximum yield) as a function of the $Z^2/A^{1/3}$ of composite systems with $Z = 82 - 120$. Circles are the data from present work; stars are the data from Ref. [20,22,30,32,33].

the TKE is lower than the Viola TKE for CN fission, while for energies above the barrier the TKE is higher. A similar behavior of TKE of symmetric fragments has been earlier observed in the reactions ^{36}S $+^{238}$U and ^{58}Fe $+^{208}$Pb in Ref. [24]. As opposed to the TKE of symmetric fragments, the average TKE of QFasym practically does not change with the collision energy. It means that the full dissipation of initial energy occurs in QFasym process and the energy excess introduced into the system transforms to intrinsic excitation of the fragments as in case of CN fission. Similarly to CN fission the TKE for QFasym process also depends linearly on the parameter $(Z_p + Z_t)^2/(A_p + A_t)^{1/3}$. The average TKEs for asymmetric QF (corresponding to the fragments with the maximum yield) as a function of the $(Z_p + Z_t)^2/(A_p + A_t)^{1/3}$ of composite systems with $Z = 82–120$ are shown in Fig. 8. The data from Refs. [20,22,30,32,33] measured with CORSET setup are also included in Fig. 8. The line is a fit to the experimental data. In spite of the fact that QFasym is determined by different neutron and proton closed shells for superheavy composite systems and for systems with $Z \sim 80$, the TKE of QFasym fragments has the same dependence on the parameter $(Z_p + Z_t)^2/(A_p + A_t)^{1/3}$. So, the TKE for QFasym fragments may be fitted as:

$$\langle \text{TKE} \rangle_{\text{QFasym}} = 39.43 + 0.085 \frac{(Z_p + Z_t)^2}{(A_p + A_t)^{1/3}}. \quad (2)$$

The standard deviation σ_{TKE} for QFasym is about 18–19 MeV for all the studied reactions, whereas for CN fission the value of ~ 22 MeV is expected. For the composite systems ^{202}Pb and ^{218}Ra σ_{TKE} for QFasym is ~ 9 MeV. Thereby the dispersion of TKE for the QFasym increases with increasing charge number of composite system and is comparable with the dispersion for the CN fission.

One may speculate about the presence of other processes together with the CN fission in the symmetric mass region for the ^{48}Ca $+^{238}$U, ^{244}Pu, and ^{248}Cm reactions. We assume that the mass symmetric fragments may be formed by three different modes: CN fission, symmetric QF, and a tail of
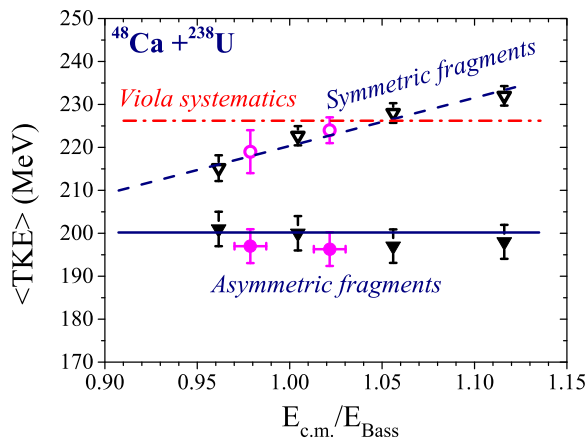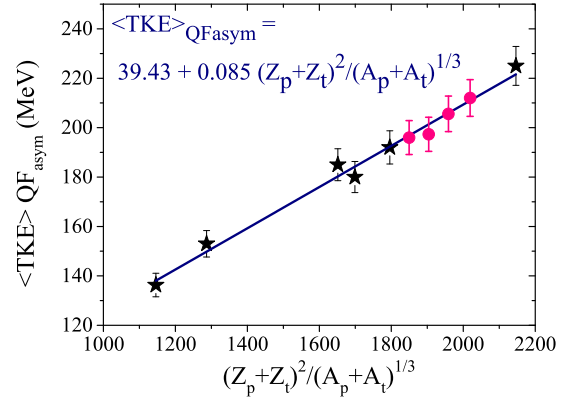

FIG. 7. (Color online) The average TKEs for asymmetric fragments corresponding to the fragments with the maximum yield (solid symbols) and symmetric fragments with masses $A_{CN}/2 \pm 20$ u (open symbols) as a function of the collision energy for the reaction ^{48}Ca $+^{238}$U. Circles are the data from present work; triangles are from Ref. [22].
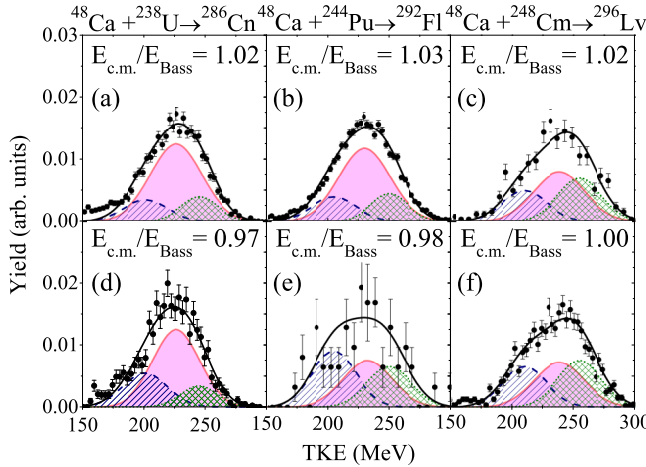
FIG. 9. (Color online) TKE distributions of fragments with masses $A_{CN}/2 \pm 20$ u for the reactions $^{48}Ca + ^{238}$U, ^{244}Pu, and ^{248}Cm. The filled region corresponds to the TKE distribution for the CN fission. The dashed and dotted curves are associated with asymmetric and symmetric QF, respectively.

asymmetric QF process. To evaluate the contribution of the CN-fission process in the symmetric mass region the TKE distributions are decomposed as a sum of three Gaussians. One of them is associated with the CN-fission process (filled region in Fig. 9). We fix the mean value and variance of this component to the values obtained from the systematics presented in Refs. [28] and [3], respectively. The low-energy component in Fig. 9 is attributed to QFasym while the high-energy one is connected with QFsym. As it was shown in Ref. [24] in the case of reaction $^{58}Fe + ^{208}$Pb (where the asymmetric quasifission is a main process even in symmetric mass region of fragments) the variance of TKE for QF does not depend on the mass of the quasifission fragments. At the fitting procedure we also fix the variance of QFasym component equal to the variance of TKE for the maximum yield of QFasym. Such descriptions of energy distributions allow us to
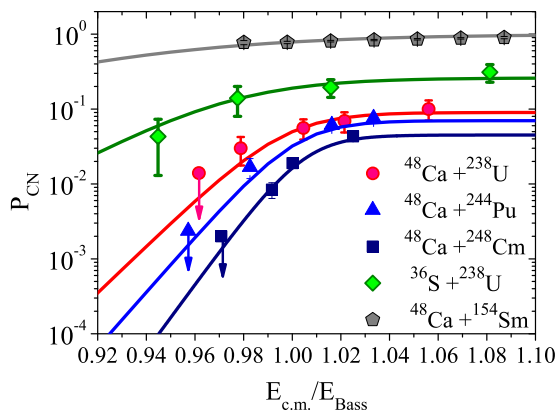

FIG. 10. (Color online) The fusion probabilities in the reactions $^{48}Ca + ^{238}$U, ^{244}Pu and ^{248}Cm obtained from the present analysis of mass-energy distributions of fissionlike reaction products in comparison with the fusion probabilities in the reactions $^{36}S + ^{238}$U from Ref. [24] and $^{48}Ca + ^{154}$Sm from Ref. [20]. The solid lines are the results of the fitting of the fusion probabilities with Eq. (3).

TABLE II. Empirical constants for the P_{CN} in Eq. (3)

Reaction	P_0	α	β
$^{48}Ca + ^{238}$U	0.09	72	0.997
$^{48}Ca + ^{244}$Pu	0.07	85	1.002
$^{48}Ca + ^{248}$Cm	0.05	102	1.005
$^{36}S + ^{238}$U	0.27	40	0.975
$^{48}Ca + ^{154}$Sm	1.00	20	0.935

explain the increase of the energy of the symmetric fragments with increasing collision energy, while for asymmetric ones it remains practically unchanged. As it can be seen from the decomposition, the contributions of CN fission and QFsym (both processes have larger TKE of fragments) increase with the increase of incident energy. Therefore, when the energy of the symmetric fragments is smaller than the Viola systematics, the asymmetric QF process dominates even in the region of symmetric fragments and leads to the reduction of TKE. In any case, a significant part of fissionlike fragments has features close to CN fission in the region of symmetric mass split. Nevertheless, going from ^{238}U to ^{248}Cm, the low energy part connected with QFasym becomes more pronounced in TKE distributions and the contribution of CN fission to the region $A_{CN}/2 \pm 20$ u decreases in the case of the reaction $^{48}Ca + ^{248}$Cm.

P_{CN} is defined as the probability for CN formation from the configuration of two nuclei in contact. As it was mentioned above, the cross section of the evaporation residues is approximately a few picobarns for these reactions. Thus we can estimate the fusion probability using the measured mass-energy distributions as the ratio between the number of events attributed to CN fission in the framework of the present analysis and all fissionlike fragments. In Fig. 10 the fusion probabilities as a function of the energy above the Bass barrier for the studied reactions are compared with the fusion probabilities for the reactions $^{36}S + ^{238}$U and $^{48}Ca + ^{154}$Sm.

To describe the dependence of P_{CN} on the interacting energy we have modified the equation for fusion probability for cold fusion reactions suggested by Zagrebaev [34]:

$$P_{CN}(E_{c.m.}) = \frac{P_0}{1 + \exp\left[\alpha\left(\beta - \frac{E_{c.m.}}{E_{Bass}}\right)\right]}, \quad (3)$$

where P_0, α and β are empirical constants. The results of the fitting of the fusion probabilities with Eq. (3) are shown as solid lines in Fig. 10. The fitted parameters are listed in Table II. The differences between the estimated values of P_{CN} and the results of the fitting procedure are typically 2–5% and do not exceed 10%.

VI. CAPTURE, FISSION, AND ER CROSS SECTIONS

The absolute differential cross sections for all fissionlike events observed in the reactions $^{48}Ca + ^{244}$Pu and ^{248}Cm were measured at the angle $\theta_{c.m.} \approx 90°$ and at energies near the Coulomb barrier. Capture cross sections σ_{cap} for all fissionlike events were estimated assuming that the angular distribution is proportional to $1/\sin\theta_{c.m.}$ This procedure seemed the most

TABLE III. Survival probabilities of Cn, Fl, and Lv compound nuclei after three and four neutron evaporations at the CN excitation energies of about 40 MeV.

CN	E_{CN}^* (MeV)	σ_{ff} (mb)	σ_{ER} (pb)	W_{sur}^{exp}
^{286}Cn*	35 ± 2	$\leqslant 4.2$	$2.5_{-1.1}^{+1.8}(3n)$	$\geqslant 6 \times 10^{-10}$
	39 ± 2	$\leqslant 9.2$	$0.6_{-0.5}^{+1.6}(4n)$	$\geqslant 7 \times 10^{-11}$
^{292}Fl*	35 ± 2	$\leqslant 2.2$	$0.5_{-0.3}^{+0.6}(3n)$	$\geqslant 2 \times 10^{-10}$
	40 ± 2	$\leqslant 6.0$	$3.6_{-1.7}^{+3.4}(3n)$	$\geqslant 6 \times 10^{-10}$
	40 ± 2	$\leqslant 6.0$	$4.6_{-1.9}^{+3.6}(4n)$	$\geqslant 7 \times 10^{-10}$
^{296}Lv*	32 ± 2	$\leqslant 0.7$	$0.5_{-0.3}^{+0.5}(3n)$	$\geqslant 7 \times 10^{-10}$
	32 ± 2	$\leqslant 0.7$	$\geqslant 0.3(4n)$	$\geqslant 4 \times 10^{-10}$
	39 ± 2	$\leqslant 4.0$	$1.2_{-0.8}^{+1.7}(3n)$	$\geqslant 3 \times 10^{-10}$
	39 ± 2	$\leqslant 4.0$	$3.2_{-1.2}^{+2.0}(4n)$	$\geqslant 8 \times 10^{-10}$

reasonable since detailed angular distributions are not available at present, as well as any model (theory) for the angular distribution of fragments produced in the QF process.

In Fig. 11 the measured capture cross sections are shown together with ER cross sections measured in FLNR taken from Ref. [1]. The capture cross section for the ^{48}Ca $+^{238}$U reaction is taken from Refs. [22,27]. The coupled channel calculations performed with NRV code [18] are shown. The cross sections for the formation of symmetric fragments with masses $A_{CN}/2 \pm 20$ u as well as CN-fission cross section σ_{ff} estimated from the analysis of TKE distribution described above are also presented in Fig. 11.

The CN-fission cross sections and ER cross section allow us to estimate the survival probability as

$$W_{sur} = \frac{\sigma_{ER}}{(\sigma_{ER} + \sigma_{ff})}. \tag{4}$$

The experimental survival probabilities estimated with Eq. (4) are listed in Table III. On the other hand the survival probability W_{sur} can be written as

$$W_{sur} = P_{xn}(E^*) \prod_{i=1}^{x} \left(\frac{\Gamma_n}{\Gamma_n + \Gamma_f} \right)_{i,E^*}, \tag{5}$$

where P_{xn} is the probability of emitting exactly x neutrons [35], the index i is equal to the number of emitted neutrons, E^* is excitation energy of CN. The evaporation of each neutron reduces the excitation energy of CN by the neutron binding energy B_n and an assumed neutron kinetic energy of $2T$ where $T = \sqrt{E^*/1.5a_n}$ is the average nuclear temperature, which is assumed to be approximately constant during the entire evaporation process. In our estimation we assume that the fission barrier B_f is the same for different isotopes of CN. According to the classical formalism from Vandenbosch [36]:

$$\frac{\Gamma_n}{\Gamma_f} = \frac{4A_{CN}^{2/3} a_f (E^* - B_n)}{k a_n \left[2a_f^{1/2}(E^* - B_f^*)^{1/2} - 1 \right]}$$
$$\times \exp \left[2a_n^{1/2}(E^* - B_n)^{1/2} - 2a_f^{1/2}(E^* - B_f^*)^{1/2} \right], \tag{6}$$
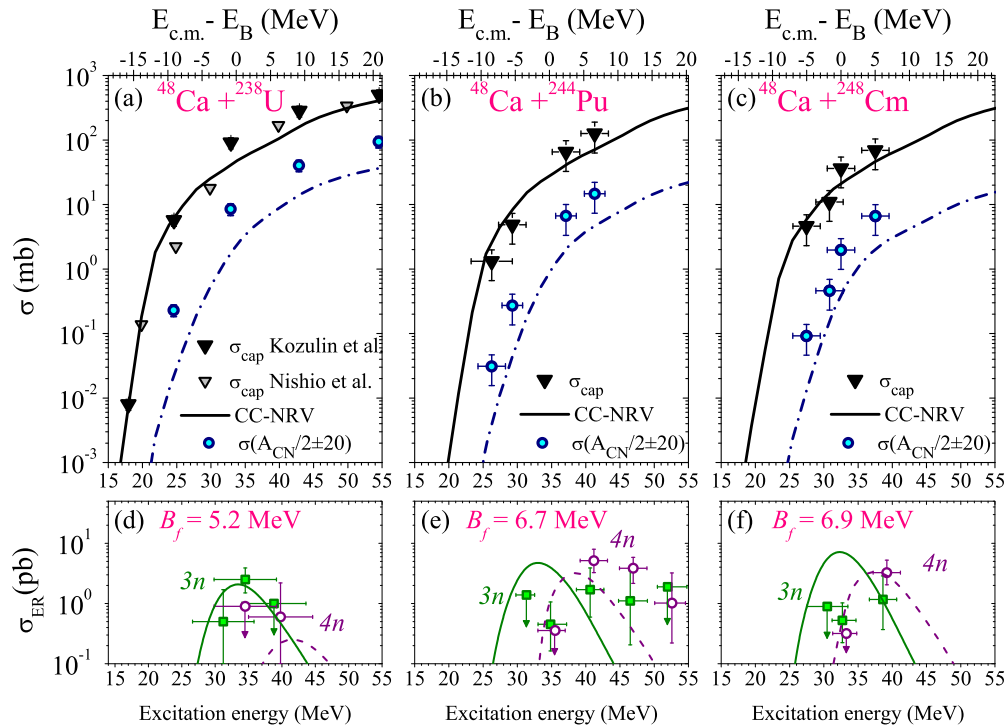

FIG. 11. (Color online) Top: Triangles are the cross sections for fissionlike fragments of the reactions ^{48}Ca$+^{238}$U [22,27], ^{48}Ca$+^{244}$Pu and ^{248}Cm. Solid lines are the coupled channel calculations. Circles are the cross sections for fragments with masses $A_{CN}/2 \pm 20$ u, the dashed-dotted lines are estimated CN-fission cross sections σ_{ff}. Bottom: excitation functions for $3n$ (squares) and $4n$ (circles) evaporation channels taken from Ref. [1]. Solid and dotted curves are the ER cross sections for the $3n$ and $4n$ channels, respectively, evaluated using the values of σ_{ff} obtained in the present work.

where $B_f^* = B_f(E^*) = B_f \exp(-\frac{E^*}{E_D})$, $a_n = A_{CN}/10, a_f = 1.1a_n, E_D = 0.4A_{CN}^{4/3}/a_n$ [37], A_{CN} is a mass number of CN.

Thus, using the obtained estimates for the survival probability for Cn, Fl, and Lv compound nuclei we may extract the height of fission barrier. We have used the binding energy values taken from Ref. [38] in these calculations. As it is clearly seen from Fig. 11 the maximum production cross sections of isotopes of elements Cn, Fl, and Lv have been observed for 3*n* and 4*n* channels at CN excitation energy of about 40 MeV.

Since, the cross sections σ_{ff} are only the upper limits for CN-fission cross section we may deduce the lower limits of the fission barriers of the corresponding nuclei. The obtained values of fission barriers are 5.2 MeV for Cn, 6.7 MeV for Fl, and 6.9 MeV for Lv. Nevertheless, the available experimental data on the fusion and fission of nuclei of ^{286}Cn, ^{292}Fl, and ^{296}Lv, produced in the reactions ^{48}Ca $+^{238}$ U, ^{48}Ca $+^{244}$ Pu, and ^{48}Ca $+^{248}$ Cm prove that the fission barriers of those nuclei are really quite high, which results in their relatively high stability. Our estimates of the lower limits for the fission barriers of $^{283-286}$Cn, $^{289-292}$Fl, and $^{293-296}$Lv are lower than the calculations of Möller [39], where the values of ~8 MeV for Cn and ~10 MeV for Fl and Lv were predicted and higher than the calculations of Smolańczuk [40] (~4 MeV for Cn and ~6 MeV for Fl and Lv). In the most recent calculations within the framework of the macroscopic-microscopic model of Kowal *et al.* [41] the fission barrier heights of about 4–5 MeV, 5.5–6.3 MeV, and 6–6.2 MeV, were found for Cn, Fl, and Lv, respectively. Thus, independent of absolute values, all models predict rather properly the same trend as we have obtained in the present work.

VII. CONCLUSIONS

The mass-energy distributions of binary fissionlike fragments produced in the reactions ^{48}Ca$+^{232}$Th, ^{238}U, ^{244}Pu, and ^{248}Cm have been measured at the energies close to the Coulomb barrier.

For all the reactions the main component of the distributions corresponds to asymmetrical mass division typical for asymmetric quasifission process. These quasifission fragments peak around the masses corresponding to closed neutron and proton shells. The major part of the asymmetric component fits into the region of shells with $Z = 28, 82$ and $N = 50, 126$. The position of the peak of heavy quasifission fragment moves from 206–208 u for the reaction ^{48}Ca $+^{232}$ Th to 210–212 u for the reaction ^{48}Ca $+^{248}$ Cm due to the shells influence in light fragment $Z_L = 28$ and $N_L = 50$. The TKE of asymmetric quasifission fragments does not depend on the collision energy and increases linearly with increasing $(Z_p + Z_t)^2/(A_p + A_t)^{1/3}$ similarly to CN-fission process.

Nevertheless, in all the reactions the contributions of symmetric fragments into all fissionlike events is of the order of several percent and increases with the interacting energy. The TKE distributions for symmetric fragments with masses $A_{CN}/2 \pm 20$ u were analyzed for all reactions studied. It was found that a significant part of the symmetric fragments have typical values of the variance and mean total kinetic energies, which are inherent in CN fission.

From the analysis of mass and TKE distributions the fusion probabilities have been estimated. At the transition from ^{238}U to ^{248}Cm the P_{CN} decreases more than two times. It was found that P_{CN} is strongly suppressed in the subbarrier region. From the measured capture cross sections for the ^{48}Ca $+^{244}$ Pu and ^{48}Ca $+^{248}$ Cm the lower limits for survival probabilities of ~10^{-10} for Fl and Lv compound nuclei have been found.

[1] Yu. Ts. Oganessian *et al.*, Phys. Rev. C **70**, 064609 (2004).

[2] U. Brosa, S. Grossmann, and A. Müller, Phys. Rep. **197**, 167 (1990).

[3] M. G. Itkis and A. Ya. Russanov, Phys. Part. Nucl. **29**, 160 (1998).

[4] J. Randrup, P. Möller, and A. J. Sierk, Phys. Rev. C **84**, 034613 (2011).

[5] J. Randrup and P. Möller, Phys. Rev. C **88**, 064606 (2013).

[6] Y. Aritomo and S. Chiba, Phys. Rev. C **88**, 044614 (2013).

[7] V. Zagrebaev and W. Greiner, J. Phys. G: Nucl. Part. Phys. **31**, 825 (2005).

[8] Y. Aritomo, K. Hagino, K. Nishio, and S. Chiba, Phys. Rev. C **85**, 044614 (2012).

[9] C. Simenel, Eur. Phys. J. A **48**, 152 (2012).

[10] W. Q. Shen *et al.*, Phys. Rev. C **36**, 115 (1987).

[11] R. Bock *et al.*, Nucl. Phys. A **388**, 334 (1982).

[12] J. Töke *et al.*, Nucl. Phys. A **440**, 327 (1985).

[13] B. B. Back, S. Bjornholm, T. Dossing, W. Q. Shen, K. D. Hildenbrand, A. Gobbi, and S. P. Sorensen, Phys. Rev. C **41**, 1495 (1990).

[14] B. B. Back *et al.*, Phys. Rev. C **53**, 1734 (1996).

[15] R. Yanez, W. Loveland, J. S. Barrett, L. Yao, B. B. Back, S. Zhu, and T. L. Khoo, Phys. Rev. C **88**, 014606 (2013).

[16] R. du Rietz *et al.*, Phys. Rev. Lett. **106**, 052701 (2011).

[17] E. M. Kozulin *et al.*, Instrum. Exp. Tech. **51**, 44 (2008).

[18] http://nrv.jinr.ru/nrv.

[19] S. Raman, C. W. Nestor, Jr., and P. Tikkanen, At. Data Nucl. Data Tables **78**, 1 (2001).

[20] G. N. Knyazheva *et al.*, Phys. Rev. C **75**, 064602 (2007).

[21] E. V. Prokhorova *et al.*, Nucl. Phys. A **802**, 45 (2008).

[22] E. M. Kozulin *et al.*, Phys. Lett. B **686**, 227 (2010).

[23] C. Simenel, D. J. Hinde, R. du Rietz, M. Dasgupta, M. Evers, C. J. Lin, D. H. Luong, and A. Wakhle, Phys. Lett. B **710**, 607 (2012).

[24] I. M. Itkis *et al.*, Phys. Rev. C **83**, 064613 (2011).

[25] G. N. Knyazheva, A. A. Bogachev, I. M. Itkis, M. G. Itkis, and E. M. Kozulin, in *Proceedings of the International Symposium on Exotic Nuclei (EXON 2009), Sochi, Russia*, edited by Yu. E. Penionzhkevich and S. M. Lukyanov (AIP, Melville, New York, 2009); AIP Conf. Proc. **1224**, 377 (2010).

[26] F. Gönnenwein, *The Nuclear Fission Process* (CRC Press, Boca Raton, Florida, 1991), Chap. 8, p. 287.

[27] K. Nishio *et al.*, Phys. Rev. C **86**, 034608 (2012).

[28] V. E. Viola, K. Kwiatkowski, and M. Walker, Phys. Rev. C **31**, 1550 (1985).

[29] J. R. Nix and W. J. Swiatecki, Nucl. Phys. **71**, 1 (1965).

[30] A. Yu. Chizhov *et al.*, Phys. Rev. C **67**, 011603 (2003).

[31] S. I. Mulgin, V. N. Okolovich, and S. V. Zhdanov, Phys. Lett. B **462**, 29 (1999).

[32] G. N. Knyazheva *et al.*, Phys. Part. Nucl. Lett. **5**, 21 (2008).

[33] M. G. Itkis *et al.*, Nucl. Phys. A **787**, 150c (2007).

[34] V. I. Zagrebaev, Y. Aritomo, M. G. Itkis, Yu. Ts. Oganessian, and M. Ohta, Phys. Rev. C **65**, 014607 (2001).

[35] J. D. Jackson, Can. J. Phys. **34**, 767 (1956).

[36] R. Vandenbosch and J. R. Huizenga, *Nuclear Fission* (Academic, New York, 1973), p. 323.

[37] K. H. Schmidt, H. Delagrange, J. P. Dufour, N. Carjan, and A. Fleury, Z. Phys. A **308**, 215 (1982).

[38] P. Möller, J. R. Nix, W. D. Myers, and W. J. Swiatecki, At. Data Nucl. Data Tabl. **59**, 185 (1995).

[39] P. Möller, A. J. Sierk, T. Ichikawa, A. Iwamoto, R. Bengtsson, H. Uhrenholt, and S. Åberg, Phys. Rev. C **79**, 064304 (2009).

[40] R. Smolańczuk, J. Skalski, and A. Sobiczewski, Phys. Rev. C **52**, 1871 (1995).

[41] M. Kowal, P. Jachimowicz, and A. Sobiczewski, Phys. Rev. C **82**, 014303 (2010).